The Astrophysical Journal, 603:139–151, 2004 March 1

OGLE-2003-BLG-262: FINITE-SOURCE EFFECTS FROM A POINT-MASS LENS[1]

Jaiyul Yoo,[2] D. L. DePoy,[2] A. Gal-Yam,[3] B. S. Gaudi,[4] A. Gould,[2] C. Han,[5] Y. Lipkin,[3] D. Maoz,[3] E. O. Ofek,[3] B.-G. Park,[6] and R. W. Pogge[2]
(The μFUN Collaboration)

and

A. Udalski,[7] I. Soszyński,[7] Ł. Wyrzykowski,[7] M. Kubiak,[7] M. Szymański,[7] G. Pietrzyński,[7] O. Szewczyk,[7] and K. Żebruń[7]
(The OGLE Collaboration)
Received 2003 September 11; accepted 2003 November 10

ABSTRACT

We analyze OGLE-2003-BLG-262, a relatively short ($t_{\rm E} = 12.5 \pm 0.1$ day) microlensing event generated by a point-mass lens transiting the face of a K giant source in the Galactic bulge. We use the resulting finite-source effects to measure the angular Einstein radius, $\theta_{\rm E} = 195 \pm 17$ μas, and so constrain the lens mass to the FWHM interval $0.08 < M/M_\odot < 0.54$. The lens-source relative proper motion is $\mu_{\rm rel} = 27 \pm 2$ km s^{-1} kpc^{-1}. Both values are typical of what is expected for lenses detected toward the bulge. Despite the short duration of the event, we detect marginal evidence for a "parallax asymmetry" but argue that this is more likely to be induced by acceleration of the source, a binary lens, or possibly by statistical fluctuations. Although OGLE-2003-BLG-262 is only the second published event to date in which the lens transits the source, such events will become more common with the new OGLE-III survey in place. We therefore give a detailed account of the analysis of this event to facilitate the study of future events of this type.

Subject headings: gravitational lensing — stars: low-mass, brown dwarfs

1. INTRODUCTION

Immediately following the announcement of the first microlensing detections (Alcock et al. 1993; Aubourg et al. 1993; Udalski et al. 1993), three groups independently showed that one could measure the microlens angular Einstein radius,

$$\theta_{\rm E} = \sqrt{\kappa M \pi_{\rm rel}}, \qquad \kappa \equiv \frac{4G}{c^2\ {\rm AU}} \simeq 8\ {\rm mas}\ M_\odot^{-1}, \tag{1}$$

from the deviations on the microlensing light curve induced by the finite size of the source (Gould 1994a; Nemiroff & Wickramasinghe 1994; Witt & Mao 1994). Here M is the mass of the lens and $\pi_{\rm rel}$ is the lens-source relative parallax. Although all three considered the case of a point-mass lens passing close to or over the face of the source star, the great majority of the actual $\theta_{\rm E}$ measurements made over the ensuing decade used binary-lens events in which the source passed over the binary caustic (Albrow et al. 1999a, 2000a, 2001; Afonso et al. 2000; Alcock et al. 2000; An et al. 2002). There has been only one single-lens event for which finite-source effects have yielded a measurement of $\theta_{\rm E}$. This was the spectacular event MACHO-95-30, whose M4 III source of radius $r_* \sim 60\ R_\odot$ was transited by the lens (Alcock et al. 1997). In fact, of the more than 1000 single-lens microlensing events discovered to date, only two have a measured $\theta_{\rm E}$ by any technique. The other was the equally spectacular MACHO-LMC-5 whose source-lens relative proper motion $\mu_{\rm rel}$ was measured by directly imaging and resolving the source and the M dwarf lens 6 yr after the event (Alcock et al. 2001). The angular Einstein radius was then inferred from

$$\theta_{\rm E} = \mu_{\rm rel} t_{\rm E}, \tag{2}$$

where $t_{\rm E}$ is the Einstein crossing time, which had been measured during the event.

Measurements of $\theta_{\rm E}$ are important because they constrain the physical properties of the lens. For most events, the only measured parameter that is related to the physical properties of the lens is $t_{\rm E}$, which (from eqs. [1] and [2]) is a combination of three such properties, M, $\pi_{\rm rel}$, and $\mu_{\rm rel}$. If $\theta_{\rm E}$ is measured, one then determines $\mu_{\rm rel}$ from equation (2), and the only remaining ambiguity is between M and $\pi_{\rm rel}$ (see eq. [1]). In some cases, $\mu_{\rm rel}$ is directly of interest. For example, measurement of the proper motion of the

[1] Based in part on observations obtained with the 1.3 m Warsaw Telescope at the Las Campanas Observatory of the Carnegie Institution of Washington.
[2] Department of Astronomy, The Ohio State University, 140 West 18th Avenue, Columbus, OH 43210; jaiyul@astronomy.ohio-state.edu, depoy@astronomy.ohio-state.edu, gould@astronomy.ohio-state.edu, pogge@astronomy.ohio-state.edu.
[3] School of Physics and Astronomy and Wise Observatory, Tel Aviv University, Tel Aviv 69978, Israel; avishay@wise.tau.ac.il, yiftah@wise.tau.ac.il, dani@wise.tau.ac.il, eran@wise.tau.ac.il.
[4] Harvard-Smithsonian Center for Astrophysics, 60 Garden Street, Cambridge, MA 02138; sgaudi@cfa.harvard.edu.
[5] Department of Physics, Institute for Basic Science Research, Chungbuk National University, Chongju 361-763, Korea; cheongho@astroph.chungbuk.ac.kr.
[6] Korea Astronomical Observatory, 61-1, Whaam-Dong, Youseong-Gu, Daejeon 305-348, Korea; bgpark@boao.re.kr.
[7] Warsaw University Observatory, Al. Ujazdowskie 4, 00-478 Warszawa, Poland; udalski@astrouw.edu.pl, soszynsk@astrouw.edu.pl, wyrzykow@astrouw.edu.pl, mk@astrouw.edu.pl, msz@astrouw.edu.pl, pietrzyn@astrouw.edu.pl, szewczyk@astrouw.edu.pl, zebrun@astrouw.edu.pl.

binary event MACHO-98-SMC-1 led to the conclusion that the lens was in the SMC itself rather than the Galactic halo (Afonso et al. 2000).

In other cases, one can combine the measurement of $\theta_{\rm E}$ with other measurements or limits to further constrain the character of the lens. The most dramatic example of this would be measurement of the microlens parallax,

$$\pi_{\rm E} = \sqrt{\frac{\pi_{\rm rel}}{\kappa M}}, \tag{3}$$

which can be determined either by observing the event from a satellite in solar orbit (Refsdal 1966; Gould 1995) or from the distortion of the microlens light curve induced by the accelerated motion of the Earth (Gould 1992; Alcock et al. 1995). If both $\theta_{\rm E}$ and $\pi_{\rm E}$ are measured, one completely solves the event, that is,

$$M = \frac{\theta_{\rm E}^2}{\kappa \pi_{\rm rel}}, \qquad \pi_{\rm rel} = \theta_{\rm E}\pi_{\rm E}. \tag{4}$$

Unfortunately, while $\pi_{\rm E}$ has been measured for about a dozen events, only one of these also has a firm measurement of $\theta_{\rm E}$ (An et al. 2002), although Smith, Mao, & Woźniak (2003b) also obtained tentative measurements of both $\theta_{\rm E}$ and $\pi_{\rm E}$.

Another type of constraint that can be combined with a measurement of $\theta_{\rm E}$ is an upper limit on the lens flux, which can often be obtained from the light curve. This flux limit can be converted into a luminosity limit at each possible lens distance. If the lens is assumed to be a main-sequence star, then using equation (1) and some reasonable assumption about the source distance, one can put an upper limit on the lens mass (e.g., Albrow et al. 2000b). Even in the absence of any additional constraints, equation (1) can be combined with a Galactic model to make statistical statements about the lens properties (e.g., Alcock et al. 1997).

The principal reason that most $\theta_{\rm E}$ measurements come from binary lenses and that single-lens measurements are extremely rare is that the ratio ρ of the angular source radius θ_* to the Einstein radius,

$$\rho \equiv \frac{\theta_*}{\theta_{\rm E}}, \tag{5}$$

is usually extremely small. At the distance of the Galactic bulge, even a clump giant has an angular radius $\theta_* \sim 6\ \mu$as, and main-sequence stars are an order of magnitude smaller. By contrast, typical Einstein radii are $\theta_{\rm E} \sim 310\ \mu{\rm as}[(M/0.3\ M_\odot)(\pi_{\rm rel}/40\ \mu{\rm as})]^{1/2}$. Hence, the probability that the lens will pass directly over the source, which is what is required for substantial finite-source effects (Gould & Welch 1996), is very small. By contrast, binary lenses, with their extended caustic structures, have a much higher probability of generating finite-source effects.

However, new microlensing surveys are beginning to alter this situation. In particular, the new phase of the Optical Gravitational Lensing Experiment, OGLE-III (Udalski et al. 2002a), with its dedicated 1.3 m telescope and new $35' \times 35'$ field, 0\".26 pixel, mosaic CCD camera and generally excellent image quality, is generating microlensing alerts at the rate of 500 per season (as reported by the OGLE-III Early Warning System[8] [EWS]), roughly an order of magnitude higher than previous surveys. This high event rate is itself enough to overcome the low, $\mathcal{O}(\rho)$, probability of a source-crossing event and hence to generate a few finite-source affected EWS alerts per year. Moreover, because EWS relies on image subtraction (Woźniak 2000), it is sensitive to extremely high magnification events of relatively faint sources, which have a higher chance of a source crossing than do typical events.

OGLE-III is able to generate this high event rate only by reducing its visits to individual fields below one per night. Hence, it would not customarily observe the alerted event during the lens transit of the source. However, several groups, including the Probing Lensing Anomalies NETwork (PLANET; Albrow et al. 1998), the Microlensing Planet Search (MPS; Rhie et al. 1999), and the Microlensing Follow-Up Network[9] (μFUN), intensively monitor alerts from EWS and also from the Microlensing Observations in Astrophysics collaboration (MOA; Bond et al. 2001), primarily to search for planets. High-magnification events are the most sensitive to planetary perturbations (Gould & Loeb 1992; Griest & Safizadeh 1998), so these groups tend to focus on these events, particularly their peaks. As a consequence, there is a good chance they will detect finite-source effects when they occur. Moreover, OGLE-III diverts time from its regular field rotation (survey mode) to especially interesting events (follow-up mode) and so can itself also directly detect these effects.

Here we report observations of EWS alert OGLE-2003-BLG-262, which exhibited clear indications of finite-source effects near its peak on 2003 July 19. By fitting this event to a single-lens finite-source model, we measure the $\theta_{\rm E}$ and hence $\mu_{\rm rel}$. We use this information, combined with a measurement of $t_{\rm E}$, to constrain the mass of the lens. We also present marginal ($\gtrsim 3\ \sigma$) evidence for an asymmetry that, if due to parallax effects, would imply that the lens was a brown dwarf. However, we argue that the observed asymmetry is due to either statistical fluctuations, a weak binary lens, or acceleration of the source. Our analysis provides a framework in which to analyze future finite-source single-lens events, which should be considerably more common as a result of the higher rate of alerted events.

2. OBSERVATIONAL DATA

The microlensing event OGLE-2003-BLG-262 was identified by the OGLE-III EWS (Udalski et al. 1994) on 2003 June 26, i.e., more than 3 weeks before peak, which occurred on ${\rm HJD}' \equiv {\rm HJD} - 2,450,000 = 2839.84$ over the Pacific Ocean. OGLE-III observations were carried out with the 1.3 m Warsaw Telescope at the Las Campanas Observatory, Chile, which is operated by the

[8] See http://www.astrouw.edu.pl/~ogle/ogle3/ews/ews.html.
[9] See http://www.astronomy.ohio-state.edu/~microfun.

Carnegie Institution of Washington. These comprise a total of 170 observations in I band, including 68 in the 2001 and 2002 seasons. The exposures were generally the standard 120 s, except for three special 40 s exposures on the peak and following night when the star was too bright for the standard exposure time. Photometry was obtained with the OGLE-III image subtraction technique data pipeline (Udalski et al. 2002a) based in part on the Woźniak (2000) DIA implementation. The source had also been monitored by OGLE-II and was found to be very stable over four previous seasons (1997 April–2000 October).

Following the alert, the event was monitored by μFUN from sites in Chile and Israel. The Chile observations were carried out at the 1.3 m (ex-2MASS) telescope at the Cerro Tololo Inter-American Observatory, using the ANDICAM, which simultaneously images at optical and infrared wavelengths (DePoy et al. 2003). During the seven nights from HJD′ 2838.5 to 2844.8, there were a total of 45 observations in I, four in V, and 28 in H. The I and V observations were generally 300 s, although the exposures were shortened to 120 s during the three nights from 2839.6 to 2841.8. The individual H observations were 60 s and were grouped in five dithered exposures, which were taken simultaneously with one 300 s V or I exposure or with two 120 s I exposures. All images were flat-fielded using sky flats for V and I and dome flats for H. Photometry was obtained with DoPHOT (Schechter, Mateo, & Saha 1993) for all V, I, and H images.

After reductions, the contiguous groups of five (or 10 in the case of back-to-back V and I exposures) H points were averaged into single data points to yield the above-stated 28 points.

The μFUN Israel observations were carried out on the Wise 1 m telescope at Mitzpe Ramon, 200 km south of Tel Aviv, roughly 105° east of Chile. During the nights of $\sim$2839.3, $\sim$2841.3, and $\sim$2842.3, there were a total of four observations in I and three in V. The exposures (all 240 s) were obtained using the Wise Tektronix 1K CCD camera. Data were flat-fielded and zero corrected in the usual way, and photometry was obtained with DoPHOT.

The position of the source is R.A. $= 17^{\mathrm{h}}57^{\mathrm{m}}08\overset{\mathrm{s}}{.}51$, decl. $= -30°20'05\overset{''}{.}1$ (J2000.0) $(l, b = 0\overset{\circ}{.}41918,\ -3\overset{\circ}{.}46935)$ and so was accessible for most of the nights near peak from Chile but only for a few hours from Israel. Unfortunately, because of a communications mixup, μFUN Chile observations on the peak night were bunched in a narrow time interval. Happily, when these are combined with the two OGLE observations, the one I-band observation, and the one V-band μFUN Israel observation, the rising half of the peak is still clearly traced out (see Fig. 1).

We emphasize that while three of the data sets have relatively few points, two of these small data sets actually play crucial roles. The three postpeak μFUN Israel I points serve to align this data set with the two larger I data sets and so enable the first point (on 2839.38) to directly test the near-peak finite-source profile, which otherwise would be determined by a single compact set of points (see Fig. 1). The four μFUN Chile V points allow determination of the color of the source and so permit one to estimate the source size and thus the proper motion and angular Einstein radius (see § 4). With only three points, two of which are nearly coincident, the μFUN Israel V data do not contribute significantly to the fit because they are absorbed by two fitting parameters, F_s and F_b. However, they are included here for completeness.

The source lies in one of the OGLE-II calibrated photometry fields[10] (Udalski et al. 2002b), and this allows us to place it on a calibrated color-magnitude diagram (CMD; see Fig. 2). The source lies on the red giant branch, about 1 mag brighter than the clump and about 0.2 mag redder. It therefore has considerably larger angular radius than typical microlens sources, and this, together with the high magnification of the event, considerably increased the chance for significant finite-source effects.

Sumi et al. (2004) measured the proper motion of the source (relative to the frame of the Galactic bulge) and found $(\mu_{\alpha,s}, \mu_{\delta,s}) = (0.45 \pm 0.41,\ -5.75 \pm 0.40)$ mas yr^{-1}. When corrected to the Tycho-2 frame, this becomes $(\mu_{\alpha,s}, \mu_{\delta,s}) = (-2.9,\ -12.4)$ mas yr^{-1}.

3. FORMALISM

3.1. *Finite-Source Effects*

In most cases, the lensed star is regarded as a point source because the angular size of the source is negligibly small compared to the angular separation of the source and the lens. The magnification is then given by (Paczyński 1986)

$$A(u) = \frac{u^2 + 2}{u(u^2 + 4)^{1/2}}, \tag{6}$$

where u is the projected source-lens separation in units of the angular Einstein radius θ_{E}. However, this approximation breaks down for $u \lesssim \rho$. Finite-source effects then dominate.

If the source were of uniform brightness, the total magnification would simply be the mean magnification over the source,

$$A_{\mathrm{uni}}(u|\rho) = W_0[(u/\rho)|\rho; A(x)], \tag{7}$$

where

$$W_n[z|\rho; f(x)] \equiv \frac{1}{\pi}\int_0^{2\pi} d\theta \int_0^1 dr\, r\left(1 - r^2\right)^{n/2} f\left(\rho\sqrt{r^2 + z^2 - 2rz\cos\theta}\right). \tag{8}$$

Witt & Mao (1994) gave an exact evaluation of this expression in closed, albeit cumbersome, form. Gould (1994a) advocated a simple approximation to equation (8),

$$A_{\mathrm{uni}}(u|\rho) \simeq A(u)B_0(u/\rho), \qquad B_0(z) \equiv z\rho W_0\left[z|\rho; x^{-1}\right], \tag{9}$$

[10] See ftp://bulge.princeton.edu/ogle/ogle2/maps/bulge.

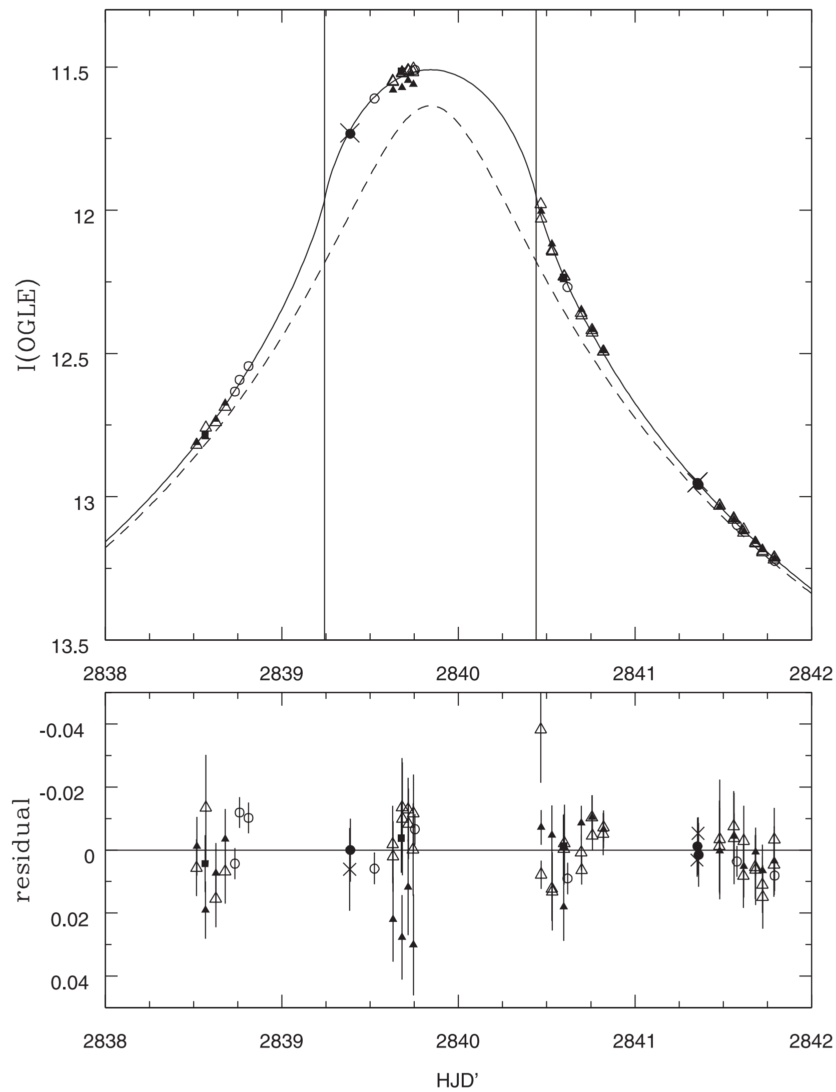

FIG. 1.—Photometry of microlensing event OGLE-2003-BLG-262 near its peak on 2003 July 19.34 (HJD 2,452,839.83). Data points are in I (OGLE: *open circles*; μFUN Chile: *open triangles*; μFUN Israel: *crosses*), V (μFUN Chile: *filled squares*; μFUN Israel: *filled circles*), and H (μFUN Chile: *filled triangles*). All bands are linearly rescaled so that F_s and F_b are the same as the OGLE observations, which define the magnitude scale. When the lens is close to or inside (vertical lines) the source, the light curves are expected to differ as a result of LD. The solid curve shows the best-fit model for the I-band curve. The fact that the H-band points near the peak are below this curve is in qualitative accord with the lower LD in H compared to I. The dashed curve shows the light curve expected for the same lens model but a point source.

which follows from the fact that $A(u) \simeq u^{-1}$ when $u \ll 1$. Note that B_0 depends on ρ only through the ratio $z = u/\rho$. However, Gould (1994a) did not explicitly evaluate B_0, nor did he demonstrate the range of validity of the approximation given by equation (9). It is straightforward to show that

$$B_0(z) = \frac{4}{\pi} z E(k, z), \qquad k \equiv \min\left(z^{-1},\ 1\right), \tag{10}$$

where E is the incomplete elliptic integral of the second kind and where we follow the notation of Gradshteyn & Ryzhik (1965). Using the expansion $A(u) = u^{-1}(1 + \frac{3}{8}u^2 + \ldots)$ and after some algebra, one may show that to second order in ρ

$$A_{\rm uni}(u|\rho) = A(u) B_0(z)\left[1 + \frac{\rho^2}{8} Q(z)\right], \qquad z \equiv \frac{u}{\rho}, \tag{11}$$

where

$$Q(z) = \frac{1}{3}\left[7 - 8z^2 - 4\left(1 - z^2\right)\frac{F(k,z)}{E(k,z)}\right], \tag{12}$$

and where F is the incomplete elliptic integral of the first kind. We find numerically that $-0.38 \le Q(z) \le 1$, where the limits are saturated at $z = 0.97$ and 0, respectively. For OGLE-2003-BLG-262, $\rho^2/8 \lesssim 5 \times 10^{-4}$, which is about an order of magnitude

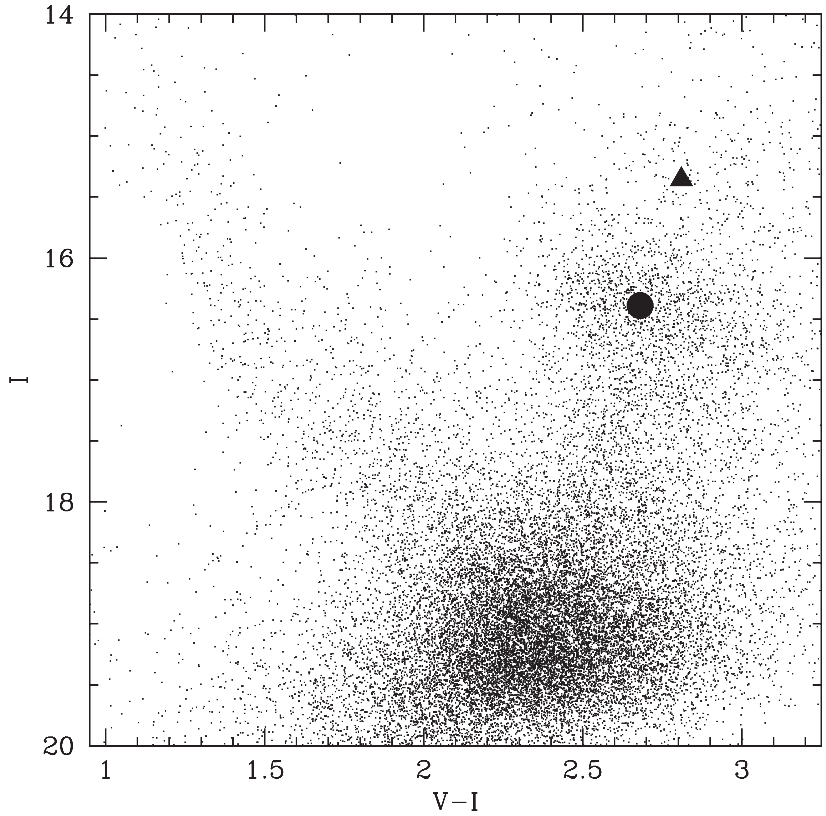

FIG. 2.—Calibrated CMD of a 10′ square around OGLE-2003-BLG-262 taken from OGLE-II photometry well before the event. The source (*filled triangle*) is about 1 mag brighter and 0.2 mag redder than the centroid of the clump giants (*filled circle*). The fit shows negligible blending, so the apparent source position on the CMD is virtually identical to its true (deblended) position.

smaller than our photometric errors. The zeroth-order approximation given by equation (9) is therefore appropriate here and, we believe, is likely to be appropriate in most other cases as well.

3.2. *Limb Darkening*

Real stars are not uniform but rather are limb-darkened. For simplicity and also because the quality of the data does not warrant a more sophisticated treatment, we adopt a one-parameter linear limb-darkening (LD) law for the surface brightness of the source,

$$S_\lambda(\vartheta) = \bar{S}_\lambda\left[1 - \Gamma_\lambda\left(1 - \frac{3}{2}\cos\vartheta\right)\right], \tag{13}$$

where ϑ is the angle between the normal to the stellar surface and the line of sight, $\bar{S}_\lambda$ is the mean surface brightness of the source, and Γ_λ is the LD coefficient for a given wavelength band λ. The factor $\frac{3}{2}$ originates from our requirement that the total flux be $F_{\mathrm{tot},\lambda} = \pi\theta_*^2\bar{S}_\lambda$.

The LD magnification is then (exactly)

$$A_{\mathrm{lld}}(u|\rho) = W_0[(u/\rho)|\rho; A(x)] - \Gamma\{W_0[(u/\rho)|\rho; A(x)] - 1.5W_1[(u/\rho)|\rho; A(x)]\}. \tag{14}$$

However, we adopt the same simplifying approximation as above and write

$$A_{\mathrm{lld}}(u|\rho) \simeq A(u)[B_0(z) - \Gamma B_1(z)], \tag{15}$$

where

$$B_1(z) = B_0(z) - \tfrac{3}{2}z\rho W_1\left(z|\rho; x^{-1}\right). \tag{16}$$

Figure 3 shows B_0, $B_{1/2}$ (see below), and B_1 as functions of z. Note that $B_0(z) \to 1$ and $B_1(z) \to 0$ in the limit $z \to \infty$ so that the magnification (eq. [15]) reduces to the point-source case. In the opposite limit, $z \to 0$, equations (10) and (16) reduce to $B_0(z) \to 2z$ and $B_1(z) \to (2 - 3\pi/4)z$, so that $A_{\mathrm{fin}}(0) = 2/\rho[1 + (3\pi/8 - 1)\Gamma]$. Hence, the peak magnification depends primarily on ρ and only weakly on Γ.

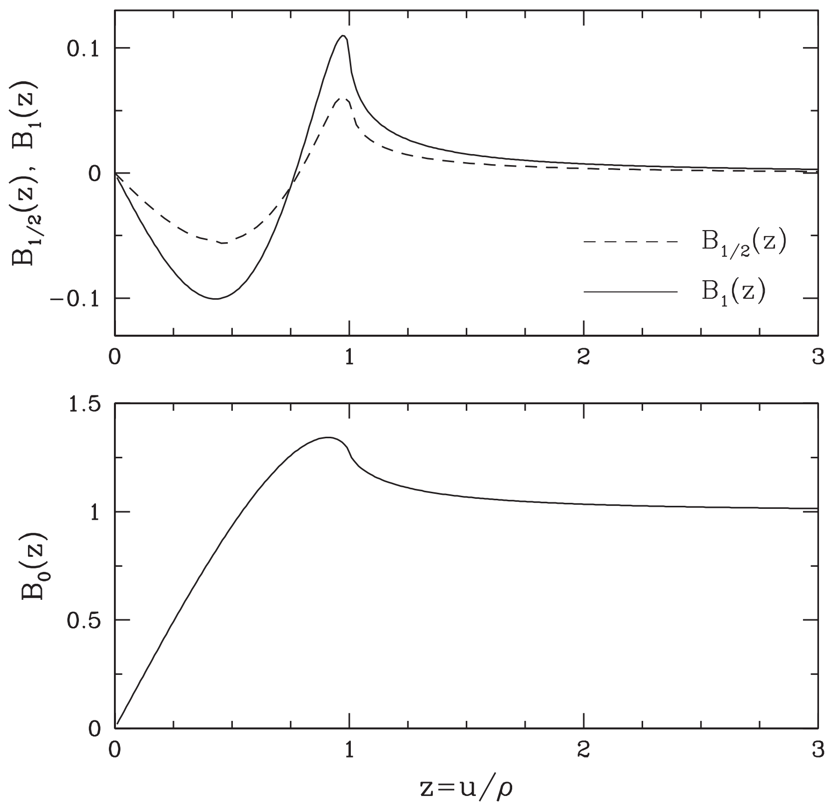

FIG. 3.—Finite-source functions $B_0(z)$, $B_{1/2}(z)$, and $B_1(z)$ given by eqs. (10), (19), and (16), respectively. For $\rho \ll 1$, the limb-darkened magnification is very well represented by $A_{\rm ld}(u|\rho) = A(u)[B_0(z) - \Gamma B_1(z)]$, where ρ is the source size and u is the lens-source separation, both in units of $\theta_{\rm E}$, Γ is the linear LD coefficient, and $z = u/\rho$.

In high-precision LD measurements, it is generally accepted that a two-parameter square root LD law is more appropriate to describe brightness profiles of stars (Albrow et al. 1999a; Fields et al. 2003) than equation (13) although it is not used in the present work. Therefore, for completeness we extend the above formalism to a two-parameter square root LD law in the form of

$$S_\lambda(\vartheta) = \bar{S}_\lambda\left[1 - \Gamma_\lambda\left(1 - \frac{3}{2}\cos\vartheta\right) - \Lambda_\lambda\left(1 - \frac{5}{4}\cos^{1/2}\vartheta\right)\right], \tag{17}$$

where Λ_λ is the additional LD coefficient for a given wavelength band λ. The magnification can then be approximated by

$$A_{\rm sqrtld}(u|\rho) \simeq A(u)\left[B_0(z) - \Gamma B_1(z) - \Lambda B_{1/2}(z)\right], \tag{18}$$

where

$$B_{1/2}(z) = B_0(z) - \frac{5}{4}z\rho W_{1/2}\left(z|\rho; x^{-1}\right). \tag{19}$$

3.3. *Parallax Effects*

Microlensing events are fitted to

$$F(t) = F_s A[u(t)] + F_b, \tag{20}$$

where F_s is the source flux, F_b is the blended background light, and

$$u(t) = \sqrt{[\tau(t)]^2 + [\beta(t)]^2}. \tag{21}$$

Conventionally, rectilinear motion is assumed,

$$\tau(t) = \frac{t - t_0}{t_{\rm E}}, \qquad \beta(t) = u_0. \tag{22}$$

Hence, the simplest fit has five parameters, F_s, F_b, the impact parameter u_0, the time of closest approach t_0, and the Einstein timescale t_E. However, even if the source and lens are in rectilinear motion, the Earth is not. Thus, strictly speaking one should write

$$\tau(t) = \frac{t - t_0}{t_\mathrm{E}} + \pi_{\mathrm{E},\parallel} a_\parallel(t) + \pi_{\mathrm{E},\perp} a_\perp(t), \tag{23}$$

$$\beta(t) = u_0 - \pi_{\mathrm{E},\parallel} a_\perp(t) + \pi_{\mathrm{E},\perp} a_\parallel(t). \tag{24}$$

Here $\boldsymbol{a} \equiv (a_\parallel, a_\perp)$ is the difference in the Earth's position (projected onto the plane of the sky and measured in AU) relative to what it would have been had the Earth maintained the velocity it had had at t_0, and the $a_\parallel$ direction is defined by the direction of the Earth's (projected) acceleration at t_0.

Choosing the Earth frame at the peak of the event as the inertial frame is certainly not standard procedure. It is more common, and mathematically more convenient, to use the Sun's frame. However, for relatively short events $t_\mathrm{E} \lesssim \mathrm{yr}/2\pi$, the parallax effect is quite weak, and it is only possible to measure one component of $\boldsymbol{\pi}_\mathrm{E} = (\pi_{\mathrm{E},\parallel}, \pi_{\mathrm{E},\perp})$, namely, the parallax asymmetry, which is the component ($\pi_{\mathrm{E},\parallel}$) of the parallax parallel to the Earth's projected acceleration at the peak of the event (Gould, Miralda-Escudé, & Bahcall 1994). In this case, u_0, t_0, and t_E as seen from the Earth at the event peak are very well defined by the fit to the event without parallax, whereas these quantities as seen from the Sun are impossible to determine. For these short events, $a_\perp \sim 0$, and the impact of $a_\parallel$ through β is undetectable because it is absorbed into u_0, t_E, F_s, and F_b. Equations (23) and (24) then reduce to

$$\tau(t) = \frac{t - t_0}{t_\mathrm{E}} + \pi_{\mathrm{E},\parallel} a_\parallel(t), \qquad \beta(t) = u_0. \tag{25}$$

4. MODEL FITTING

We begin by fitting the event taking account of both LD and parallax. There are then a total of 20 free parameters: 12 parameters for F_s and F_b from each of the six observatory/filter combinations; three LD parameters, one each for *I*, *V*, and *H*, the basic microlensing parameters t_0, u_0, and t_E; and the source size, ρ, and the parallel component of the parallax, $\pi_{\mathrm{E},\parallel}$. We consider the possibility of a correction for seeing but find no correlation of the residuals of the μFUN Chile *I* or *H* data with seeing. The source is quite bright (see Fig. 2) and is virtually unblended (see below), so it is quite plausible that there would be no seeing correlations. We set a minimum error of 0.003 mag for all observations, regardless of what value the photometry programs report. We then rescale the errors for the OGLE, μFUN Chile *I*, and *H* by factors of 1.62, 1.12, and 1.83, respectively, in order to force χ^2/dof to unity. There are too few points in each of the remaining observatory/filter combinations to permit accurate rescalings, and the actual total χ^2 values for these are consistent with the reported errors being correct.

We minimize χ^2 using Newton's method (e.g., Press et al. 1992), which guarantees that one has found a local minimum because the derivative of χ^2 with respect to each parameter is zero. In contrast to caustic-crossing binary lenses (Albrow et al. 1999b; Dominik 1998) and to space-based (Gould 1994b; Refsdal 1966) and ground-based (Smith, Mao, & Paczyński 2003a) parallax measurements for which there can be multiple local minima, standard microlensing (even when modified by inclusion of finite-source effects) is expected to have a single global minimum. We nevertheless checked for multiple minima by adopting several initial trial solutions that were consistent with point-source/point-lens fits to a data set that excluded the peak. All converged to the same solution.

We initially allow the three LD coefficients to be free parameters. We find fit values and errors $(\Gamma_V, \Gamma_I, \Gamma_H) = (0.85 \pm 0.21,\ 0.61 \pm 0.15,\ 0.10 \pm 0.20)$ (see Table 1). These errors are all relatively large. The values therefore appear only mildly inconsistent with those of EROS-BLG-2000-5, $(\Gamma_V, \Gamma_I, \Gamma_H) = (0.72,\ 0.44,\ 0.26)$ (Fields et al. 2003), a slightly redder source with much better measured LD. It is then somewhat shocking to discover that there is a net penalty of $\Delta\chi^2 = 19$ for enforcing the EROS-BLG-2000-5 LD values. A major part of the problem is that while the errors in the individual LD parameters are large, the data strongly demand a large LD *difference* $\Delta\Gamma = \Gamma_I - \Gamma_H = 0.51 \pm 0.09$ when Γ_I is held fixed at 0.44; that is, although the errors on the individual determinations of Γ_I and Γ_H are large, they are strongly correlated, such that the difference $\Delta\Gamma$ is much better determined. This in turn can be traced to the fact that there is a color offset $\Delta(I-H) = -0.03$ at the peak, which is clearly visible in Figure 1 and which the fitting routine ascribes to the source having much more LD in *I* than *H* and hence being relatively blue in the center (see Fig. 4). However, since the measurement seems to contradict what is otherwise known about LD and derives primarily from a single cluster of data points, which may be subject to common systematic error, we choose to fix the three Γ-values at the above-stated EROS-BLG-2000-5 values. We thereby lose any independent LD information. This is not a major loss since our errors are too large to be competitive with other measurements (e.g., Fields et al. 2003). Our main concern is that whatever problem may be corrupting the LD could also impact the measurement of the parameters that we are most interested in measuring, which are principally ρ and t_E. In fact, by enforcing these Γ-values, ρ is changed by only 1.6% and t_E by only 0.3%. Since enforcing the LD parameters has no practical consequences (other than the loss of LD information), we adopt the EROS-BLG-2000-5 value.

We then find

$$\rho = 0.0599 \pm 0.0005, \qquad t_\mathrm{E} = 12.557 \pm 0.094\ \text{days}. \tag{26}$$

Figure 1 shows the fit to the data in the region of the peak. All six observatory/band combinations have been linearly rescaled to have an F_s and F_b equal to those of the OGLE data set. The three *I*-band data streams should then follow the same light curve, whose best-fit model is shown by the solid curve. However, the *V*- and *H*-band points should deviate from this curve during the

TABLE 1
OGLE-2003-BLG-262 Fit Parameters

Parameter	Free Fit Value	Free Fit Error	Fixed LD Value	Fixed LD Error	Fixed LD and π_E Value	Fixed LD and π_E Error
t_0 (days)........	2839.8411	0.0015	2839.8415	0.0015	2839.8424	0.0014
u_0.................	0.0365	0.0005	0.0362	0.0004	0.0360	0.0004
t_E (days).......	12.5309	0.0945	12.5568	0.0941	12.6181	0.0916
ρ..................	0.0605	0.0010	0.0599	0.0005	0.0595	0.0005
Γ_V................	0.8515	0.2069	0.7200	...	0.7200	...
Γ_I.................	0.6118	0.1499	0.4400	...	0.4400	...
Γ_H................	0.0975	0.2028	0.2600	...	0.2600	...
$\pi_{E,\parallel}$...............	−0.8572	0.3130	−0.8335	0.3120	0.0000	...
$(F_b/F_s)_{I_1}$......	−0.0011	0.0095	0.0028	0.0093	0.0083	0.0091
$(F_b/F_s)_{I_2}$......	−0.0275	0.0175	−0.0134	0.0172	−0.0027	0.0168
$(F_b/F_s)_{I_3}$......	0.1865	0.0783	0.2283	0.0746	0.2361	0.0749
$(F_b/F_s)_{V_2}$.....	0.0122	0.0481	0.0192	0.0478	0.0296	0.0479
$(F_b/F_s)_{V_3}$.....	0.0406	0.1688	0.1251	0.1465	0.1191	0.1473
$(F_b/F_s)_H$......	−0.0048	0.0176	−0.0114	0.0175	−0.0009	0.0172
χ^2.................	233.50	...	252.66	...	259.76	...

Note.—Observatories: 1 = OGLE; 2 = μFUN Chile; 3 = μFUN Israel.

source crossing, $|t - t_0| \lesssim \rho t_e = 0.76$ days, because of LD. There are not enough data in the V band to test this. As mentioned above, the H-band cluster of points near the peak clearly lies below the curve, probably by too much.

We measure a parallax asymmetry,

$$\pi_{E,\parallel} = 0.83 \pm 0.31. \tag{27}$$

In other words, parallax is formally detected at the 3 σ level. More specifically, $\Delta\chi^2 = 7$ relative to enforcing $\pi_{E,\parallel} = 0$. To illustrate the strength (or lack thereof) of this detection, we show in Figure 5 the fit to the data enforcing $\pi_{E,\parallel} = 0$. The bottom panel of this figure shows the residuals together with their expected form for $\pi_{E,\parallel} = 1$. When we first constructed this figure on about

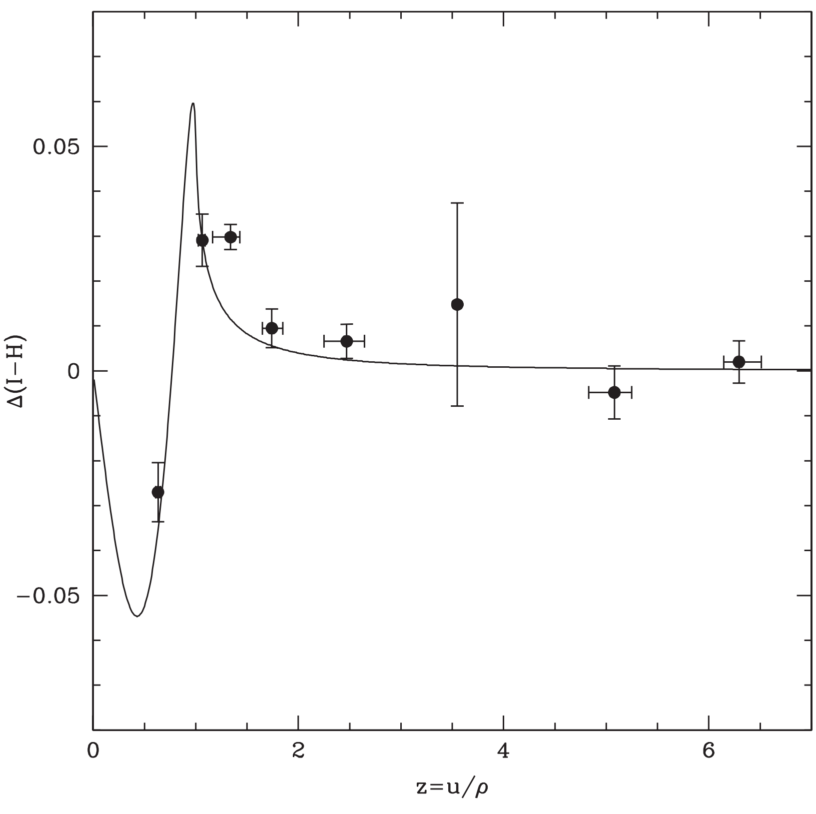

Fig. 4.—Model-independent color changes due to LD. A linear regression of H on I flux is performed at high z ($z > 1.7$) to put the two passbands on the same scale and to remove the small blending difference. Then I−H is measured at each point and the measurements for each day are averaged, except for HJD′ ∼ 2840.5 ($z \sim 1.25$), which is broken into two bins. The curve is $0.5B_1(z)$, which is the expected form of this magnitude difference for a linear LD difference $\Gamma_I - \Gamma_H = 0.5$.

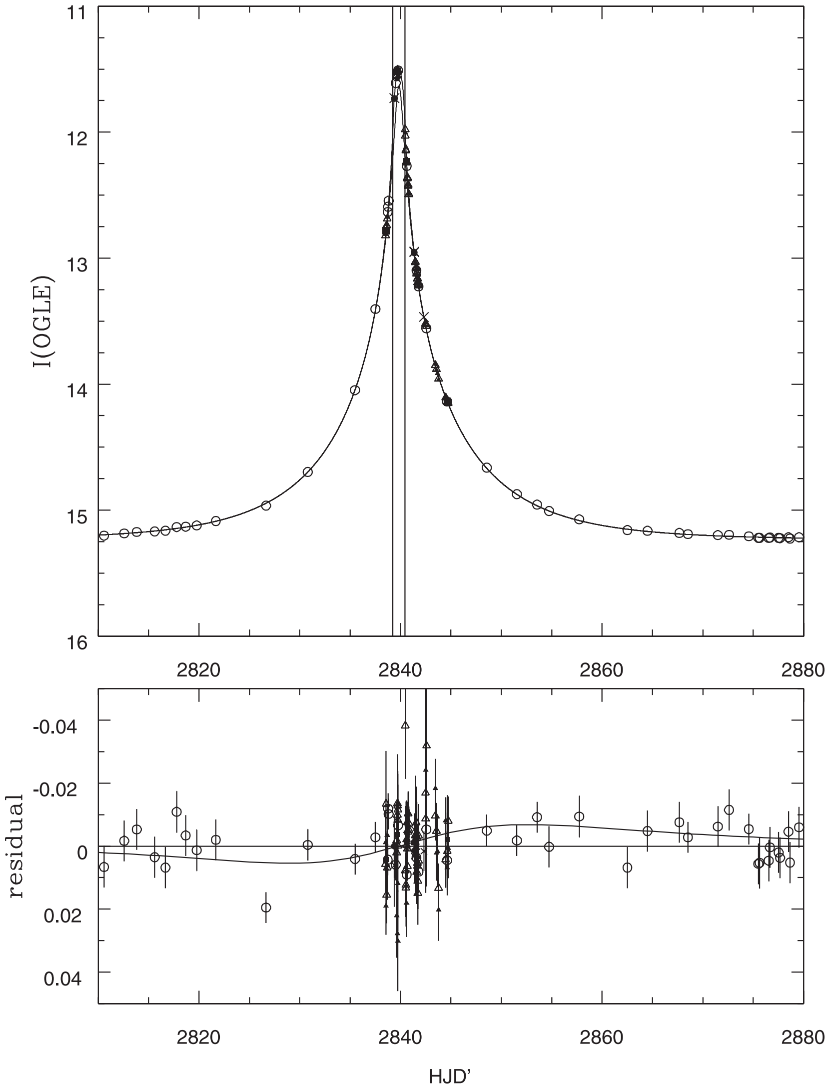

FIG. 5.—Similar to Fig. 1, but now a full view of the light curve of OGLE-2003-BLG-262 over about five Einstein timescales. The fit does not include parallax, and the residuals (*bottom panel*) show an asymmetry such as would be induced by acceleration of the Earth parallel to the direction of lens motion (*solid curve*).

HJD$' = 2870$, we realized that there might still be time to test the reality of this parallax detection. OGLE observations were then intensified from one every several days to one or two per day. These additional observations did not tend to confirm the detection but also did not firmly contradict it. Hence, the parallax detection remains ambiguous. All previous events with firm parallax detections had Einstein timescales at least 5 times longer than this one, so it would have been remarkable if we had obtained a robust detection. Moreover, as we discuss in § 6, the sign of the effect is opposite to what would be produced by the expected lens-source kinematics, while the effect itself could be produced by xallarap or by lens binarity.

The errors shown in Table 1 are $c_{ii}^{1/2}$, where c_{ij} is the ijth element of covariant matrix, and the correlation coefficients defined as $\tilde{c}_{ij} \equiv c_{ij}/c_{ii}^{1/2} c_{jj}^{1/2}$ are

$$\begin{pmatrix} 1.0000 & 0.2000 & -0.0675 & -0.1441 & 0.2288 & 0.1139 & -0.1137 \\ 0.2000 & 1.0000 & -0.8463 & 0.7969 & -0.1861 & 0.8972 & -0.8971 \\ -0.0675 & -0.8463 & 1.0000 & -0.9244 & 0.2790 & -0.9793 & 0.9758 \\ -0.1441 & 0.7969 & -0.9244 & 1.0000 & -0.2990 & 0.9086 & -0.9060 \\ 0.2288 & -0.1861 & 0.2790 & -0.2990 & 1.0000 & -0.2467 & 0.2531 \\ 0.1139 & 0.8972 & -0.9793 & 0.9086 & -0.2467 & 1.0000 & -0.9986 \\ -0.1137 & -0.8971 & 0.9758 & -0.9060 & 0.2531 & -0.9986 & 1.0000 \end{pmatrix}, \quad (28)$$

where parameters are t_0, u_0, $t_{\rm E}$, ρ, $\pi_{{\rm E},\parallel}$, $(F_s)_{I_1}$, and $(F_b)_{I_1}$. As expected from experience with standard microlensing events, F_s and F_b are extremely correlated, and these are both highly correlated with u_0 and $t_{\rm E}$. What is new in equation (28) is that ρ is also highly correlated with these other four parameters. The fundamental reason for this is that all five of these parameters are symmetric in $(t - t_0)$. By contrast, $\pi_{\mathrm{E},\parallel}$ is only weakly correlated with the other parameters.

5. CONSTRAINTS ON THE EVENT

5.1. *Angular Einstein Radius θ_E*

As discussed by Albrow et al. (2000a), one can determine θ_* from the source's dereddened color and magnitude $[(V-I)_0, I_0]_s$ by first transforming from $(V-I)_0$ to $(V-K)_0$ using the color-color relations of Bessell & Brett (1988) and then applying the empirical relation between color and surface brightness to obtain θ_* (van Belle 1999).

Again following Albrow et al. (2000a), we determine $[(V-I)_0, I_0]_s$ from the measured offset of the unamplified source (as determined from the microlensing fit) relative to the centroid of the clump giants on an instrumental CMD, the latter's dereddened color and magnitude being regarded as "known." We measure this offset to be

$$\Delta I = I_s - I_{\mathrm{clump}} = -1.06, \qquad \Delta(V-I) = (V-I)_s - (V-I)_{\mathrm{clump}} = 0.15. \tag{29}$$

In general, the source may be blended, so that the V and I of the source derived from the microlensing fit will not necessarily agree with those of the object identified as the "source" in an image taken at baseline. Hence, one cannot in general derive the offset from a CMD constructed from such a baseline image. However, in this case, there is essentially no blending, so the offset in the baseline-calibrated CMD shown in Figure 2 is virtually identical (within 0.02 mag) to that given in equation (29).

The "known" values of $[(V-I)_0, I_0]_{\mathrm{clump}}$ have recently come under dispute. The basic problem is that the previous calibrations of these quantities relied on a number of steps, in each of which it was assumed that the ratio of total to selective extinction was $R_{VI} \equiv A_V/E(V-I) \sim 2.5$. However, using this same value, Paczyński (1998) and Stutz, Popowski, & Gould (1999) found, respectively, that the colors of bulge clump giants and RR Lyrae stars were anomalous relative to local populations. Popowski (2000) then proposed that these anomalies could be resolved if the dust toward this line of sight were itself anomalous, with $R_{VI} \sim 2.1$. Udalski (2003) then demonstrated that this was very likely the case based on OGLE-II data. While it would be both worthwhile and feasible to retrace all the steps that led to the old calibration in light of this revised R_{VI}, the magnitude of this project lies well beyond the scope of the present work. Pending such a revision, we adopt a simpler approach.

The distance to the Galactic center has now been measured geometrically by Eisenhauer et al. (2003) to be $R_0 = 8.0 \pm 0.4$ kpc based on the "visual-binary" method of Salim & Gould (1999). Bulge stars are of similar metallicity to local stars, so the clump should be of similar color to the *Hipparcos* clump stars $(V-I)_0 \sim 1.00$. (Recall that it was the apparent failure of this expectation that led to the discovery of anomalous extinction.) The I-band luminosity of clump stars does not depend strongly on age (until the stars are so young that the turnoff luminosity approaches that of the horizontal branch). Hence, the bulge clump stars should have approximately the same M_I as the *Hipparcos* sample. For this we adopt $M_I = -0.20$, the value found by Paczyński & Stanek (1998) for their 70 pc sample (and prior to their reddening correction, which we consider to be substantially too large). Hence, in lieu of a more thoroughgoing calibration, we adopt

$$[(V-I)_0, I_0]_{\mathrm{clump}} = (1.00,\ 14.32). \tag{30}$$

Combining equations (29) and (30) and applying the van Belle (1999) relation, we find

$$\theta_* = 11.7 \pm 1.0\ \mu\mathrm{as}, \tag{31}$$

where the error comes primarily from the 8.7% intrinsic scatter in the van Belle (1999) relation.

This evaluation would appear to depend on the assumption that the source suffers exactly as much extinction as a typical clump star, which it might not, as a result of either highly variable extinction or the source lying well in the foreground and so in front of a large fraction of the dust. In fact, if it were determined that the extinction toward the source were greater than to the clump by $\Delta E(V-I) = 0.2$ or less by $\Delta E(V-I) = -0.6$, the estimate of θ_* would change less than 3%. This is because the changes in the inferred surface brightness and luminosity lead to changes in the source-size estimate that go in opposite directions.

Combining equations (26) and (31), we obtain

$$\theta_{\mathrm{E}} = 195 \pm 17\ \mu\mathrm{as}, \qquad \mu_{\mathrm{rel}} = 5.63 \pm 0.49\ \mathrm{mas\ yr^{-1}} = 26.7 \pm 2.3\ \mathrm{km\ s^{-1}\ kpc^{-1}}. \tag{32}$$

We now use this measurement of θ_{E}, in conjunction with its definition, equation (1), to write the source-lens relative parallax as a function of the lens mass,

$$\pi_{\mathrm{rel}}(M) = \frac{\theta_{\mathrm{E}}^2}{\kappa M} = 4.8\ \mu\mathrm{as}\left(\frac{M}{M_\odot}\right)^{-1}. \tag{33}$$

Given a Galactic mass model along the line of sight, $\rho(x)$, the prior probability of a given relative parallax is proportional to

$$P(\pi_{\mathrm{rel}}) \propto \int_0^\infty dD_s\, D_s^2 \rho(D_s) \int_0^{D_s} dD_l\, D_l \rho(D_l)\, \delta\left[\pi_{\mathrm{rel}} - \left(\frac{\mathrm{AU}}{D_l} - \frac{\mathrm{AU}}{D_s}\right)\right], \tag{34}$$

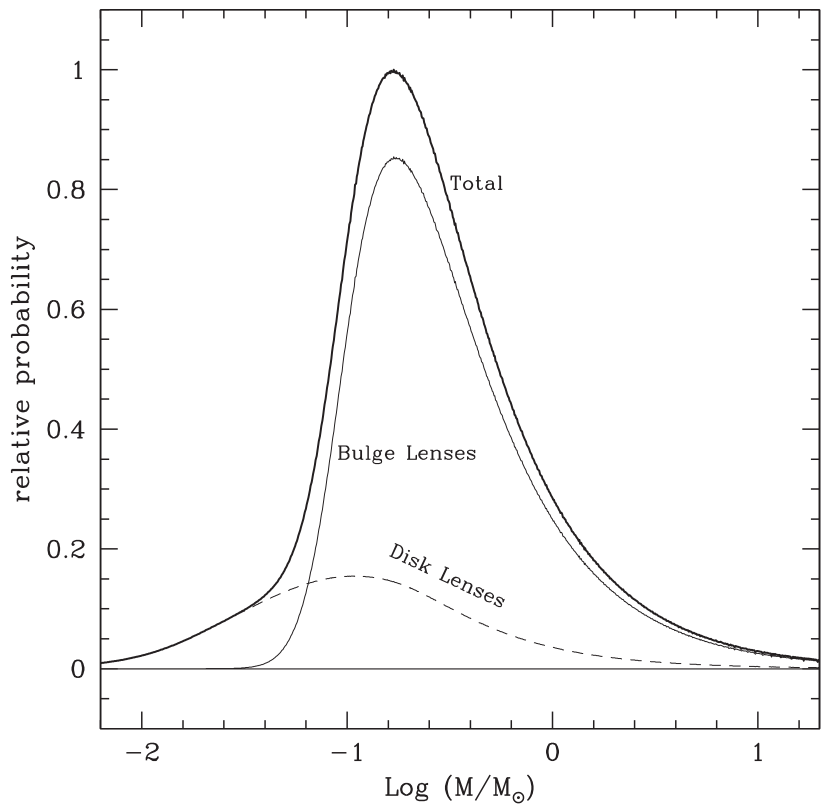

Fig. 6.—Constraints on the lens mass of OGLE-2003-BLG-262. The curves show the relative probability of different lens masses given the measurement of $\theta_{\rm E} = 195$ μas and the mass distribution along the line of sight as predicted by the Han & Gould (1995, 2003) model. The solid and dashed curves show the probability for bulge-bulge and disk-bulge combinations, respectively, of lenses and sources. The thick curve is their sum. The constraints arising from the determination of $\mu_{\rm rel}$ (equivalently $t_{\rm E}$) would be extremely weak and are not incorporated here.

where D_l and D_s are the lens and source distances, respectively. We adopt the Han & Gould (1995, 2003) model, and in Figure 6 we plot $\pi_{\rm rel}(M)P[\pi_{\rm rel}(M)]$ versus $\log M$ to display the constraint placed on the mass by the measurement of $\theta_{\rm E}$. The FWHM range is

$$\log{(M/M_\odot)} = -0.7 \pm 0.4 \text{ (FWHM)}. \qquad (35)$$

In the absence of such a measurement, the only constraint comes from the measurement of $t_{\rm E}$, and this is extremely weak, having an FWHM of a factor of $\sim$100 (see Fig. 1 from Gould 2000). Indeed, as shown in that figure, the mere supposition that the lens is a star places stronger constraints on the lens mass than does the measurement of $t_{\rm E}$.

The measurements of $\theta_{\rm E}$ and $t_{\rm E}$ yield $\mu_{\rm rel}$ (eq. [2]). Since the distribution of $\mu_{\rm rel}$ varies with D_l and D_s, one could in principle use its determination (eq. [32]) to place further constraints on combinations of these parameters and hence (through eq. [33]) on the mass. In practice, for bulge sources, the distribution of $\mu_{\rm rel}$ hardly varies as a function of lens position, even when one considers bulge versus disk lenses. Moreover, the actual measured value of $\mu_{\rm rel}$ is near the peak of that distribution. Hence, we do not incorporate this constraint.

The $\mu_{\rm rel}$ measurement does effectively rule out a foreground disk source. (Without this constraint, i.e., from the CMD alone, the source could plausibly be a disk clump giant at $D_s \sim 5$ kpc.) However, for disk-disk events along this line of sight, the observer, lens, and source all share the same transverse motion as a result of the flat rotation curve of the Galaxy. Hence, only their peculiar motions relative to this rotation enter $\mu_{\rm rel}$, and these are only of order tens of kilometers per second. Hence, $\mu_{\rm rel}$ would be only a few kilometers per second per kiloparsec, much slower than the measured value.

The Sumi et al. (2004) proper-motion measurement of the source independently rules out a foreground disk lens, since the source is moving roughly opposite to the direction of Galactic rotation at about $\mu \sim -v_c/R_0$, where $v_c \sim 220$ km s^{-1} and $R_0 = 8$ kpc. In fact, this measurement by itself would be consistent with the source lying in the background disk, behind the bulge. However, such a scenario is virtually ruled out by the CMD (see Fig. 2), which shows the source lying in or slightly above the bulge giant branch. If the source lay at, say, 10 kpc, it would intrinsically be $\sim$0.5 mag brighter still.

Combining our measurement, $\mu_{\rm rel} = 5.6$ mas yr^{-1}, with the Sumi et al. (2004) measurement, $(\mu_\alpha, \mu_\delta) = (-2.9,\ -12.3)$ mas yr^{-1}, we can effectively rule out a disk lens. These measurements imply $|\mu_L| = |\mu_s + \mu_{\rm rel}| \gtrsim 7$ mas yr^{-1}, whereas a disk lens would be expected to have roughly zero proper motion.

5.2. *Lens Luminosity $M_{I,l}$*

The measurement of the unlensed background flux, F_b, gives an upper limit to the flux from the lens. The measured background flux is a function of observatory and filter and tends to grow with larger mean seeing. Hence, the best constraint is expected to come from the observatory with the best seeing. In our case, this is OGLE. The OGLE F_b is also by far the best constrained, in part because of the large number of baseline points. The OGLE background-to-source flux ratio is $F_b/F_s = 0.003 \pm 0.009$, which yields a 3 σ lower limit on the magnitude difference of the lens and source, $I_l - I_s > 3.6$. For this limit to be at all relevant, the lens must be close to the turnoff or brighter, implying that it is close to a solar mass. Then, from equation (33), the source and lens must be nearly the same distance. This implies in turn that the above limit on apparent magnitude difference translates directly into a limit on absolute magnitude difference. Since the source is about 1 mag brighter than the clump, the constraint yields only $M_{I,l} > 2.4$, which is of very limited value.

6. MICROLENS PARALLAX $\pi_{\rm E}$

The detection of microlens parallax is marginal. We therefore begin by investigating whether its tentatively detected value is consistent with what else is known about the lens. Given this orientation and for simplicity of exposition, we ignore the very large error in the measurement. Only one component of the parallax is measured. We therefore actually have a limit, not a measurement, of $\pi_{\rm E} \geq |\pi_{{\rm E},\parallel}| = 0.86$. Together with equations (4) and (32), this implies $M \leq 0.03\ M_\odot$ and $\pi_{\rm rel} \geq 170\ \mu$as. The source distance cannot be much more than $D_s \sim 10$ kpc, partly because of the low density of stars at greater distances and partly because it would lie in an unpopulated portion of the CMD. Hence, $\pi_l = \pi_{\rm rel} + \pi_s > 270\ \mu$as, i.e., $D_l < 3.7$ kpc. In other words, the lens would be a disk brown dwarf.

Apart from the small peculiar velocity of each, the lens and Earth are both rotating about the Galactic center at the same speed. Hence, the lens should be seen moving against the bulge at about $\sim$220 km s^{-1} toward Cygnus, which is to say at a position angle roughly 30° east of north. Because the dispersion of bulge stars is about 90 km s^{-1}, this should also be approximately the direction of lens motion relative to the source.

Since only one component of $\pi_{\rm E}$ is measured, all we can test is the sign of this prediction. From the postpeak residuals to the fit without parallax (Fig. 5), the Earth is accelerating in the direction of the lens motion (thus slowing down the end of the event). On July 19 (roughly 1 month after opposition), this is basically opposite the direction of the Earth's motion and so is basically toward the west. Since the field is south of the ecliptic, there is also a small component of this (projected) acceleration toward the south. Hence, the position angle of the projected acceleration vector is about 260°, which is misaligned with the expected direction of the lens motion by about 130°; that is, the expected sign of $\pi_{{\rm E},\parallel}$ is opposite to what is expected.

While it remains possible that the peculiar velocities of the lens and source conspire to produce this result, the statistical significance of the parallax measurement is not high enough to warrant its acceptance in the face of this strong contrary expectation.

Moreover, there are at least two other possible explanations for this asymmetry apart from statistical fluctuations. The first is xallarap, distortions in the light curve due to accelerated motion of the source rather than the lens. Indeed, Smith et al. (2003a) showed that any parallax effect could be mimicked by the orbital motion of the source around an unseen companion. When both components of $\pi_{\rm E}$ are well measured, this possibility can be largely discounted because the probability of the source being in a binary with the same inclination, phase, and period as the Earth's orbit is extremely small. However, in the present case, in which all that is detected is a single component of acceleration, there is a very wide class of source binaries that could mimic the observed parallax signal. Moreover, by the arguments given in § 5.2, any source companion on the main sequence would be undetectable in the light curve (other than through its effect accelerating the source). The xallarap hypothesis could be checked by radial velocity measurements.

Still another possible source of the asymmetry is a very weak binary lens. Gaudi et al. (2002) detected a similarly weak asymmetry in OGLE-1999-BLG-36 and were able to model this with either parallax or a low-mass companion to the lens. Thus, asymmetric residuals can be attributed to several effects including parallax, xallarap, and binary lenses.

We thank Martin Smith for valuable comments on the manuscript and Dale Fields for providing us with the best-fit linear limb-darkening coefficients for EROS-BLG-2000-5. Work at Ohio State University was supported by grants AST 02-01266 from the NSF and NAG 5-10678 from NASA. B. S. G. was supported by a Menzel Fellowship from the Harvard College Observatory. C. H. was supported by the Astrophysical Research Center for the Structure and Evolution of the Cosmos (ARCSEC″) of Korea Science and Engineering Foundation (KOSEF) through Science Research Program (SRC) program. Partial support to the OGLE project was provided by the NSF grant AST 02-04908 and NASA grant NAG5-12212 to B. Paczyński and the Polish KBN grant 2P03D02124 to A. Udalski. A. U., I. S., and K. Ż. also acknowledge support from the grant "Subsydium Profesorskie" of the Foundation for Polish Science.

REFERENCES

Afonso, C., et al. 2000, ApJ, 532, 340
Albrow, M. D., et al. 1998, ApJ, 509, 687
———. 1999a, ApJ, 522, 1011
———. 1999b, ApJ, 522, 1022
———. 2000a, ApJ, 534, 894
———. 2000b, ApJ, 535, 176
———. 2001, ApJ, 549, 759
Alcock, C., et al. 1993, Nature, 365, 621
———. 1995, ApJ, 454, L125
———. 1997, ApJ, 491, 436
———. 2000, ApJ, 541, 270
———. 2001, Nature, 414, 617
An, J. H., et al. 2002, ApJ, 572, 521
Aubourg, E., et al. 1993, Nature, 365, 623
Bessell, M. S., & Brett, J. M. 1988, PASP, 100, 1134
Bond, I. A., et al. 2001, MNRAS, 327, 868
DePoy, D. L., et al. 2003, Proc. SPIE, 4841, 827
Dominik, M. 1998, A&A, 333, 893
Eisenhauer, F., Schödel, R., Genzel, R., Ott, T., Tecza, M., Abutter, R., Eckart, A., & Alexander, T. 2003, ApJ, 597, L121
Fields, D. L., et al. 2003, ApJ, 596, 1305
Gaudi, B. S., et al. 2002, ApJ, 566, 463
Gould, A. 1992, ApJ, 392, 442
———. 1994a, ApJ, 421, L71
———. 1994b, ApJ, 421, L75
———. 1995, ApJ, 441, L21

Gould, A. 2000, ApJ, 535, 928
Gould, A., & Loeb, A. 1992, ApJ, 396, 104
Gould, A., Miralda-Escudé, J., & Bahcall, J. N. 1994, ApJ, 423, L105
Gould, A., & Welch, D. L. 1996, ApJ, 464, 212
Gradshteyn, I. S., & Ryzhik, I. M. 1965, Table of Integrals Series and Products (London: Academic)
Griest, K., & Safizadeh, N. 1998, ApJ, 500, 37
Han, C., & Gould, A. 1995, ApJ, 447, 53
———. 2003, ApJ, 592, 172
Nemiroff, R. J., & Wickramasinghe, W. A. D. T. 1994, ApJ, 424, L21
Paczyński, B. 1986, ApJ, 304, 1
———. 1998, Acta Astron., 48, 405
Paczyński, B., & Stanek, K. Z. 1998, ApJ, 494, L219
Popowski, P. 2000, ApJ, 528, L9
Press, W. H., Flannery, B. P., Teukolsky, S. A., & Vetterling, W. T. 1992, Numerical Recipes (Cambridge: Cambridge Univ. Press)
Refsdal, S. 1966, MNRAS, 134, 315
Rhie, S. H., Becker, A. C., Bennett, D. P., Fragile, P. C., Johnson, B. R., King, L. J., Peterson, B. A., & Quinn, J. 1999, ApJ, 522, 1037
Salim, S., & Gould, A. 1999, ApJ, 523, 633
Schechter, P. L., Mateo, M., & Saha, A. 1993, PASP, 105, 1342
Smith, M. C., Mao, S., & Paczyński, B. 2003a, MNRAS, 339, 925
Smith, M. C., Mao, S., & Woźniak, P. 2003b, ApJ, 585, L65
Stutz, A., Popowski, P., & Gould, A. 1999, ApJ, 521, 206
Sumi, T., et al. 2004, MNRAS, in press
Udalski, A. 2003, ApJ, 590, 284
Udalski, A., Szymański, M., Kałużny, J., Kubiak, M., Mateo, M., Krzemiński, W., & Paczyński, B. 1994, Acta Astron., 44, 227
Udalski, A., et al. 1993, Acta Astron., 43, 289
———. 2002a, Acta Astron., 52, 1
———. 2002b, Acta Astron., 52, 217
van Belle, G. T. 1999, PASP, 111, 1515
Witt, H. J., & Mao, S. 1994, ApJ, 430, 505
Woźniak, P. R. 2000, Acta Astron., 50, 421